

# Probability of the emergence of helical precipitation patterns in the wake of reaction-diffusion fronts

Shibi Thomas,<sup>1,\*</sup> István Lagzi,<sup>2,†</sup> Ferenc Molnár Jr.,<sup>3,‡</sup> and Zoltán Rácz<sup>4,§</sup>

<sup>1</sup>*Department of Theoretical Physics, Eötvös University, 1117 Budapest, Hungary*

<sup>2</sup>*Department of Physics, Budapest University of Technology and Economics, 1111 Budapest, Hungary*

<sup>3</sup>*Department of Physics, Applied Physics, and Astronomy,  
Rensselaer Polytechnic Institute, 12180 Troy, NY, USA*

<sup>4</sup>*Institute for Theoretical Physics - HAS, Eötvös University, 1117 Budapest, Hungary*

(Dated: August 23, 2021)

Helical and helicoidal precipitation patterns emerging in the wake of reaction-diffusion fronts are studied. In our experiments, these chiral structures arise with well defined probabilities  $P_H$  controlled by conditions such as e.g., the initial concentration of the reagents. We develop a model which describes the observed experimental trends. The results suggest that  $P_H$  is determined by a delicate interplay among the time- and length-scales related to the front and to the unstable precipitation modes and, furthermore, the noise amplitude also plays a quantifiable role.

PACS numbers: 05.40.-a, 02.50.-r, 68.35.Ct

Helices and helicoids are present from nano- to macro-scale (ZnO nanohelices [1], macromolecules and inorganic crystals with a helical structure [2, 3], precipitation helices [4–6], fiber geometry of heart walls [7]). Formation of these fascinating structures generally follows two routes. First, templates with chiral symmetry (e.g., oragogel fibers) may exist in the system, and the symmetry is just transcribed to a structure (e.g., inorganic materials [8]) at a larger scale. Second, spontaneous symmetry breaking may occur through the self-assembly of achiral building blocks into a helical/helicoidal structure, as e.g. in case of crystals with chiral morphology [2, 9].

Theoretically, the symmetry-breaking route is more interesting. Universal aspects may emerge and the robust features of this self-organization process may be important for applications as well. Indeed, control over creating helical structures would make engineering (in particular, the bottom-up design of micro-patterns [10]) more flexible since chiral morphology of materials are known to affect their physical (electronic) properties [6, 11].

In order to develop insight into the genesis of helices/helicoids, we investigate an emblematic example of pattern formation, namely the formation of precipitation patterns in the wake of reaction-diffusion fronts [12, 13]. The motivation for this choice comes from the observation that helicoidal structures have an axis, and the correlations are simple in the plane perpendicular to the axis. This suggests that building the perpendicular correlations in the wake of an advancing planar front may be a simple and natural mechanism of creating helices/helicoids. Additional motivation comes from the existence of a large body of knowledge in the related Liesegang phenomena [12, 13]. It allows the use of well-established experimental and theoretical approaches, thus making it easier to develop a novel view on the formation of helical structures.

Our main results concern the probabilistic aspects of

the symmetry-breaking route. We determine the probability  $P_H$  of the emergence of single helices/helicoids in Liesegang-type experiments as the conditions such as the initial concentration of inner or outer electrolytes, or the temperature are changed.  $P_H$  is found to be well reproducible and large ( $P_H > 0.5$  for some parameter range). The results are understood by expanding and simulating a model of formation of precipitation patterns [14]. We explicitly observe that the origin of helices/helicoids is not to be found in the fluctuations and asymmetry of the initial- or boundary conditions [15, 16]. Instead, the growth of unstable modes, the dynamics of the front, and the bulk fluctuations (noise) combine to yield the helices.

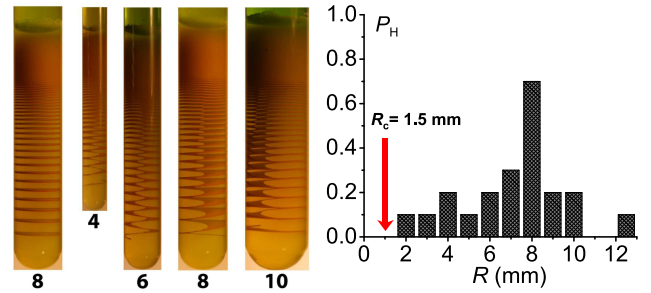


FIG. 1: Regular Liesegang- (leftmost tube) and helicoidal patterns (all other tubes) in agarose gel with the numbers corresponding to the tube radius  $R$  measured in mm.  $R$  is varied at fixed experimental conditions ( $T=22$  °C,  $[\text{Cu}^{2+}]_0=a_0=0.5$  M, and  $[\text{CrO}_4^{2-}]_0=b_0=0.01$  M) and the probability of helicoid formation  $P_H$  is displayed (right panel). No helicoid appears for  $R \leq R_c$ .

In our experiments, we study the precipitation reaction  $\text{Cu}^{2+}(\text{aq}) + \text{CrO}_4^{2-}(\text{aq}) \rightarrow \text{CuCrO}_4(\text{s})$  in 1% agarose gel. The gel soaked with  $\text{K}_2\text{CrO}_4$  (inner electrolyte) is placed in a test tube and a solution of  $\text{CuCl}_2$  (outer electrolyte) is poured on top of the gel. Setting the concentration of the outer electrolyte an order of magnitude larger than

that of the inner electrolyte yields a reaction front diffusing into the gel, and a Liesegang pattern of precipitation bands forms behind the front (Fig.1). Frequently, however, helicoids evolve from the same macroscopic experimental conditions (Fig.1). We quantified the stochastic nature of this intriguing phenomenon by varying the concentration of the outer ( $a_0$ ) and inner ( $b_0$ ) electrolytes, the radius of the test tube ( $R$ ), and the temperature ( $T$ ), and measuring  $P_H$  using 10 independent experiments for each parameter set.

Similar experiments were carried out in a quasi two-dimensional geometry as well. The gel (with the inner electrolyte  $B$ ) was placed in the gap between two test tubes of slightly different radii ( $\delta R = 2$  mm), thus effectively confining the pattern to the surface of a cylinder (Fig.2). In this geometry, we observed the formation of regular Liesegang rings, single helices, double helices, and more complex patterns for large  $R$ .

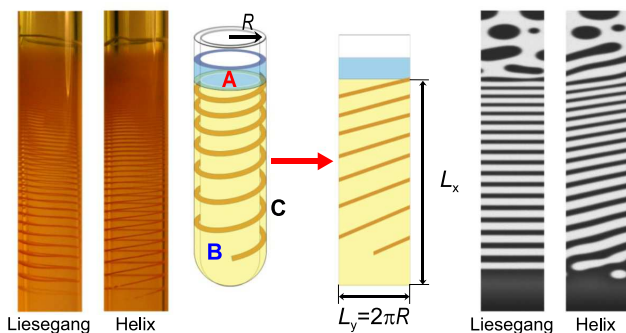


FIG. 2: Transforming the thin layer of gel in the *tube-in-tube* experiment into a two-dimensional strip. The Liesegang bands and the helices in the experiments were obtained in agarose gel at  $T = 22^\circ\text{C}$ ,  $a_0 = 0.5$  M, and  $b_0 = 0.01$  M, with the radii of the outer and inner tubes being 8 and 6 mm. The scaled parameters used for the simulations (columns on the right with the precipitate shown in white) were  $a_0 = 80$ ,  $b_0 = 1$ ,  $\sigma = 0.8$ ,  $\lambda = 0.2$ ,  $\eta = 0.05$ , and  $L_y = 64$ .

Fig.1 shows regular bands and helicoidal patterns in test tubes of various radii, together with the measured probability of helicoid formation ( $P_H$ ). We observe no helicoids below a critical radius ( $R_c = 1.5$  mm), in agreement with theoretical expectations based on a simplified model where the reaction front moves with fixed velocity [15, 16]. For  $R > R_c$ , one finds that  $P_H$  increases with increasing  $R$ , and reaches rather large values ( $P_H \approx 0.7$  at  $R = 8$  mm) before decreasing again. The decrease at large  $R$  is due to the noticeable proliferation of complex structures (double or triple helicoids, disordered patterns) which suppress the weight of single helicoids.

Before describing the experiments further, we turn to the theory since it allows a more concise discussion of the results. Theories of Liesegang-type patterns combine the properties of a moving front (i.e. where and at what rate the reaction product,  $A + B \rightarrow C$ , appears) with the

details of the precipitation (i.e. how the reaction product,  $C$ , turns into precipitate). While the front properties have been thoroughly studied and understood both theoretically [17, 18] and experimentally [19, 20], the dynamics of precipitation is more debated [13, 18]. The competing pre- and post-nucleation views can be combined [18, 21], and we shall use a simple version [14] based on the Cahn-Hilliard equation with noise added [22–24]. This equation features spinodal-decomposition-type fast dynamics, as well as slower, nucleation-and-growth processes [25]. Driving it with a reaction zone gives us a flexible model with a variety of pattern-formation regimes.

The reaction front appears due to a strongly inhomogeneous initial distribution of the reagents  $A$  and  $B$ . The reaction takes place in a gel (occupying the half space  $x > 0$ ) and, initially, the inner electrolyte  $B$  is homogeneously distributed [ $b(x > 0, y, t = 0) = b_0$ ]. The outer electrolyte  $A$  of much higher concentration [ $a(x < 0, y, t = 0) = a_0$  with  $a_0 \gg b_0$ ] is brought into contact with the gel at  $t = 0$ . Assuming a second-order irreversible reaction  $A + B \rightarrow C$ , the front invading the gel can be described by the equations

$$\partial_t a = D_A \Delta a - kab \quad (1)$$

$$\partial_t b = D_B \Delta b - kab \quad (2)$$

where both the reaction rate  $k$  and the diffusion coefficients, which are assumed to be equal ( $D_A = D_B = D$ ), are set to 1 by an appropriate choice of the time- and length-scales [26]. The front, specified in terms of the rate of production of  $C$ s ( $kab$ ), is narrow and moves into the gel diffusively (the position is given by  $x_f = \sqrt{2D_f t}$  where  $D_f$  is a function of  $D$  and  $b_0/a_0$ ). The front leaves behind a constant concentration of  $C$ s ( $c_0$ ), where  $c_0$  depends on  $D$  and  $b_0/a_0$ , and it is practically independent of  $k$ . Provided the system with  $c_0$  is unstable or metastable, a phase separation of  $C$ s into regions of high ( $c_h$ ) and low concentrations ( $c_\ell$ ) takes place. This process is described by the Cahn-Hilliard equation with source ( $kab$ ) and noise ( $\eta_c$ ) terms added

$$\partial_t m = -\lambda \Delta (m - m^3 + \sigma \Delta m) + kab + \eta_c. \quad (3)$$

Here  $m$  is the concentration of  $C$ s shifted by  $\bar{c} = (c_h + c_\ell)/2$  and scaled by  $\hat{c} = (c_h - c_\ell)/2$ , so that  $m = (c - \bar{c})/\hat{c}$  is 1 for  $c = c_h$  and  $m = -1$  for  $c = c_\ell$ . The parameters  $\lambda$  and  $\sigma$  are the rescaled kinetic coefficient and surface tension, respectively [14, 23, 24]. Their ratio  $\tau_u \approx \sigma/\lambda$  defines a characteristic timescale of the growth of unstable modes in precipitation. Comparing  $\tau_u$  with the time the front passes through a region determines whether slow nucleation-and-growth or fast spinodal decomposition dominates the pattern formation.

Adding noise ( $\eta_c$ ) is essential since the formation of helices is a symmetry-breaking process. Furthermore, the noise widens the available regions of the meta- and unstable states (see earlier morphological phase diagrams

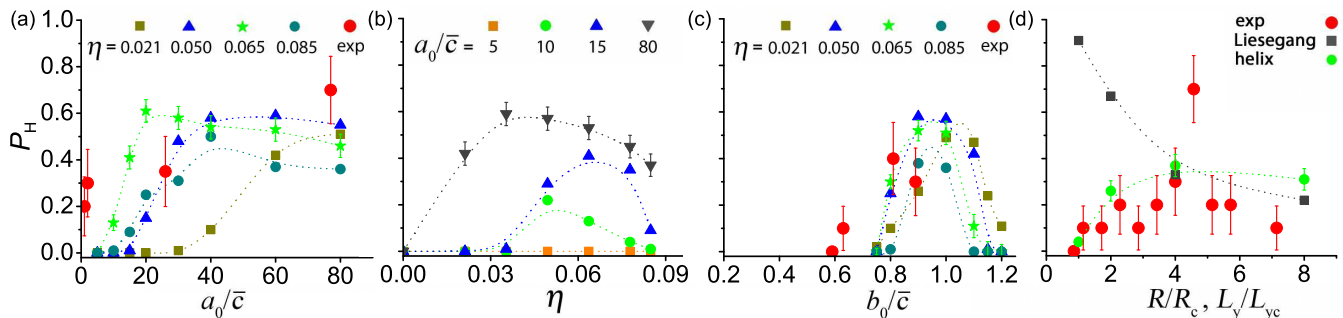


FIG. 3: The probability of helicoid/helix formation  $P_H$  in experiments (large red dots) and in simulations (small symbols). Displayed are the dependence on the outer- and inner electrolyte concentrations (Panels **a** and **c**), on the noise amplitude (**b**), and on the radius (width) of the system (**d**). The values of the parameters kept fixed in a panel, and the experimental estimate of the scale factor  $\bar{c}$  are discussed in the text. Statistical errors are shown for the experiments and for a single set of simulations.

of Liesegang patterns [27]). Noiseless Cahn-Hilliard type dynamics where the front moves with *fixed velocity* have been much studied [28, 29]. In these cases, however, noise was present in the initial state, and complex morphologies resulted from complex initial conditions or from complex motion of the reaction front. Our model without the noise reproduces the properties of the regular Liesegang patterns [14, 30]. Inclusion of the bulk noise allows us to demonstrate the existence of helices, and understand the experimental trends in their emergence.

From a theoretical point of view, the *tube-in-tube* experiments are the easiest to describe. We can cut and open the cylinder as shown in Fig.2 and treat the thin layer as a two-dimensional strip of width  $L_y = 2\pi R$ , and length equal to the tube length  $L_x$  [31]. Accordingly, eqs.(1-3) are solved in a rectangle of size  $L_x \times L_y$  with periodic boundary conditions in the  $y$  direction and no-flux boundary conditions at the lower edge ( $x = L_x, y$ ). At the upper edge (the initial location of the front ( $x = 0, y$ ), we use a slightly idealized boundary: the concentration of the outer electrolyte is kept at a constant value  $a(x = 0, y, t) = a_0/\bar{c}$  while no-flux condition is adopted for  $B$  and  $C$ . The initial conditions reflect the experimental setup:  $b(x > 0, y, t = 0) = b_0/\bar{c}$ ,  $a(x > 0, y, t = 0) = 0$ , and  $c(x, y, t = 0) = 0$ . The discretized noise term  $\eta_c$  is implemented by moving  $C$ s between neighboring sites at a rate  $\eta_c = \sqrt{c}r$  where  $r$  is uniformly distributed in the interval  $[-\eta, \eta]$ . In the following,  $\eta$  is called the amplitude of the noise.

Our simulations indicate that both the Liesegang bands and the helices emerge in a wide range of the parameters. There are, of course, some constraints, e.g.,  $\eta$  must be sufficiently small for the phase separation to take place. Examples of simulations are shown in Fig.2 (rightmost two columns), where a Liesegang pattern and a helix are displayed [26]. A general feature of the simulations is that the chirality of the helices is random within the statistical error of 100 independent simulations. This is in agreement with the experiments where, out of 96 helicoids/helices, the ratio of left- and right-handed pat-

terns is 50/46. We consider this as experimental evidence that the macroscopic symmetry breaking is not driven by microscopic objects of given chirality.

To characterize the emergence of the helices quantitatively, we collected data by varying  $a_0$ ,  $b_0$ ,  $\eta$  and  $L_y$ , and determined  $P_H$  from the outcome of 100 simulations with distinct random number sequences for  $\eta_c$ . Since the kinetic coefficients  $\lambda$  and  $\sigma$  cannot be controlled externally, we kept them fixed ( $\lambda = 0.2$ ,  $\sigma = 0.8$ ) throughout the simulations.

First, we varied  $a_0/\bar{c}$  and  $\eta$  while keeping  $b_0/\bar{c} = 1$  and  $L_y = 64$  fixed. Figs.3a,b shows that  $P_H$  is remarkably large, it increases with  $a_0$  and reaches  $P_H \sim 0.4 - 0.6$  for large  $a_0/\bar{c}$ . Similar trend is also seen in the experiments. Since  $a_0/b_0$  determines the front motion, with larger  $a_0$  corresponding to faster diffusion, an important conclusion from Fig.3a is that fast motion of the front facilitates the emergence of helices.

Fig.3a,b also show that no helices form even for larger  $a_0/\bar{c}$  if the noise is too small. Increasing the noise first increases  $P_H$ , then  $P_H$  saturates in the region  $0.05 < \eta < 0.09$  and, finally,  $P_H \rightarrow 0$  due to the absence of phase separation above  $\eta \approx 0.09$ . Comparing Fig.3b with experiments is difficult since the link between  $\eta$  and  $T$  is through complex changes in diffusion, reaction rates etc. Our experiments indicate that  $P_H$  increases with  $T$ . This is in agreement with Fig.3b provided  $\eta \sim T$  and the experimental  $T$  corresponds to small values of  $\eta$ .

We also varied  $b_0/\bar{c}$  and  $\eta$  while fixing  $a_0/\bar{c} = 80$  and  $L_y = 64$  (Fig.3c). The probability  $P_H$  was found to be maximal in the middle of the spinodal region ( $b_0/\bar{c} \approx 0.9 - 1.1$ ) where isotropic precipitation structures develop through fast-growing, linearly unstable modes. Comparing the simulations (Fig.3c) with experiments is difficult since neither  $\eta$  nor the experimental concentration scale,  $\bar{c} = (c_h + c_\ell)/2 \approx c_h/2$ , are known. We estimated  $c_h$  by assuming that all the precipitate was in the helices and all the  $B$ s reacted and turned into  $C$ s. This estimate left an apparent shift between the experimental and simulation points (Fig.3c). The shift may well be

the consequence of overestimating  $c_h$  (e.g., not all the  $B$ s reacted, or the bands are wider than their optical width).

The effect of increasing width ( $L_y$ ) is displayed in Fig.3d. The experimental parameters are described in Fig.1, while in simulations, we used  $a_0/\bar{c} = 15$ ,  $b_0/\bar{c} = 1$ , and  $\eta = 0.04$ . The experimentally observed lower threshold for the emergence of helices is clearly present ( $L_{yc} \approx 32$ ), and one can also recognize the trend that  $P_H$  first increases with  $L_y$  and then decreases for large  $L_y$ . As in experiments,  $P_H$  decreases due to the proliferation of more complex structures. Complexity builds up for large  $L_y$  since more long-wavelength transverse modes (modes in the  $y$ -direction) can fit into the system. They are unstable modes of the Cahn-Hilliard dynamics facilitating the formation of more intricate patterns.

The common trends found in experiments and simulations suggest that our model contains the right ingredients, and we can develop a physical picture of helix formation by observing the simulations. Fig.4 displays two examples of time evolutions with parameters set to have roughly equal probabilities for bands and helices. There are many ways of choosing such parameters but the characteristic features of the dynamics are always the same. Essential among them is that, initially, the reaction front moves fast enough to produce a domain where the system is unstable and roughly homogeneous (fuzzy regions in the  $t = 720 - 960$  plates in Fig.4). The homogeneity makes possible the generation of isotropic patterns which compete with the anisotropic influence of the front favoring band-formation perpendicular to the front motion ( $t = 1440 - 1920$  plates in Fig.4). The outcome of this competition determines whether Liesegang bands, single helix, double helix or more complicated patterns emerge.

One can quantify the above picture by noting that homogeneous patterns can form only if the front moves a distance of the order  $L_y$  in a time,  $\tau_f = L_y^2/2D_f$  that is smaller than the time,  $\tau_u$ , required for the precipitation to develop. To estimate  $\tau_u$ , we calculate the growth rate,  $\omega_{k^*} = \lambda/4\sigma \approx 1/\tau_u$ , of the fastest growing mode of wave-number  $k^* = 1/\sqrt{2\sigma}$  using linearized Cahn-Hilliard dynamics for a quench to the middle of the miscibility gap [ $m(0) \approx 0$ ]. Then, assuming that the homogeneous structure emerges from the noise, we have  $\sqrt{\eta} \exp(\omega_{k^*} \tau_u) \approx m(\tau_u) \approx 1$ , and the inequality  $\tau_f < \tau_u$  yields an upper limit for the width of a system  $L_y^2 < 4D_f\sigma |\ln \eta|/\lambda$  where helix can form. A lower limit can also be found since the characteristic size of the domains ( $L^* \approx 2\pi/k^* = 2\pi\sqrt{2\sigma}$ ) formed by the fastest growing modes must be smaller than the width of the system ( $L^* < L_y$ ), otherwise no structure forms in the  $y$  direction. The combination of the two inequalities

$$8\pi^2\sigma < L_y^2 < 4D_f\sigma |\ln \eta|/\lambda \quad (4)$$

reflects some of the trends observed in the experiments and simulations. Namely, the formation of helices are facilitated by a fast moving front, i.e. by  $D_f$  being large

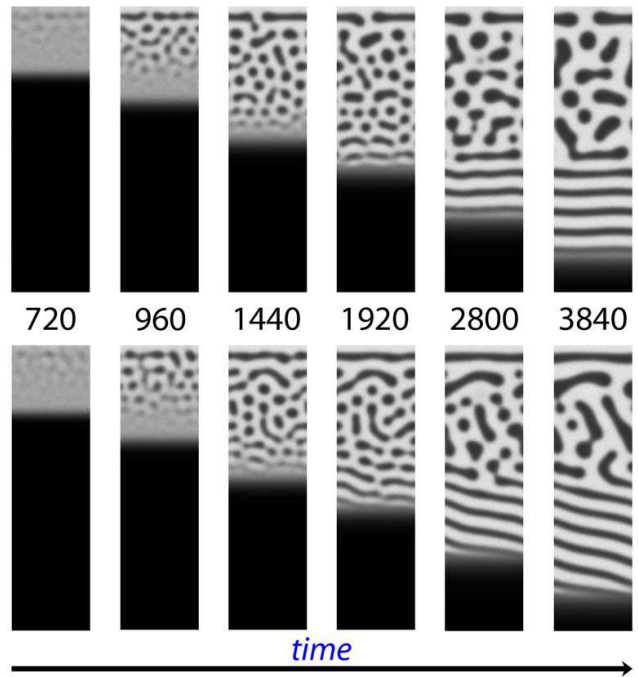


FIG. 4: Time evolution of the precipitate (white regions) for parameters  $a_0/\bar{c} = 60$ ,  $b_0/\bar{c} = 1$ ,  $\eta = 0.02$ , and  $L_y = 64$ .

which, in turn, requires  $a_0$  to be large and, furthermore, there is a minimal width below which no helices form.

Since the width ( $L_y$ ) is bounded from both sides, it may happen that no helices can form. When searching for helices one should, in general, use a fast front (e.g., by selecting large  $a_0$ ) and create an unstable state behind the front by placing the system deep in the miscibility gap (e.g., by experimenting with  $b_0$ ). Finding the right temperatures is also important but it is a rather complex problem left for future studies.

**Acknowledgments.** This work was funded by the Hungarian Academy of Sciences through OTKA Grants No. K68109, NK100296, and K104990. IL was also supported by a Magyar Postdoctoral Fellowship. FM acknowledges partial support by NSF through Grant No. DEB-0918413.

\* Present address: Department of Physics, University of Calicut, 673635 Kerala, India; Electronic address: shibithomas969@gmail.com

† Electronic address: istvanlagzi@gmail.com

‡ Electronic address: molnaf@rpi.edu

§ Electronic address: racz@general.elte.hu

- [1] P. X. Gao, Y. Ding, W. J. Mai, W. L. Hughes, C. S. Lao, and Z. L. Wang, *Science* **309**, 1700 (2005).
- [2] H. Imai, and Y. Oaki, *Angew. Chem. Int. Edit.* **43**, 1363 (2004).
- [3] D. S. Su, *Angew. Chem. Int. Edit.* **50**, 4747 (2011).

- [4] S. C. Müller, S. Kai, and J. Ross, *Science* **216**, 635 (1982).
- [5] R. V. Suganthi, E. K. Girija, S. Narayana Kalkura, H. K. Varma, and A. Rajaram, *J. Mater. Sci.- Mater. in Med.* **20**, 131 (2009).
- [6] O. Giraldo, S. L. Brock, M. Marquez, S. L. Suib, H. Hillhouse, and M. Tsapatsis, *Nature*, **405**, 38 (2000).
- [7] P. Savadjiev, G. J. Strijkers, A. J. Bakermans, E. Piuze, S. W. Zucker, and K Siddiqi, *Proc. Nat. Acad. Sci. USA*, **109**, 9248 (2012).
- [8] J. H. Jung, Y. Ono, K. Hanabusa, and S. Shinkai, *J. Am. Chem. Soc.*, **122**, 5008 (2000).
- [9] Y. Oaki and H. Imai, *J. Am. Chem. Soc.*, **126**, 9271 (2004).
- [10] B. A. Grzybowski, K. J. M. Bishop, C. J. Campbell, M. Fialkowski, and S. K. Smoukov, *Soft Matter* **1**, 114 (2005).
- [11] S. Y. Ju, J. Doll, I. Sharma, and F. Papadimitrakopoulos, *Nat. Nanotechnol.* **3**, 356 (2008).
- [12] Henisch, H. K. *Crystals in gels and Liesegang rings*, Cambridge University Press, Cambridge (1988).
- [13] S. C. Müller and J. Ross, *J. Phys. Chem. A* **107**, 7997 (2003).
- [14] T. Antal, M. Droz, J. Magnin, and Z. Rácz, *Phys. Rev. Lett.* **83**, 2880 (1999).
- [15] D. S. Chernavskii, A. A. Polezhaev, and S. C. Müller, *Physica D* **54**, 160 (1991).
- [16] A. A. Polezhaev and S. C. Müller, *Chaos*, **4** 631 (1994).
- [17] L. Gálfi and Z. Rácz, *Phys. Rev. A* **38**, 3151 (1988).
- [18] T. Antal, M. Droz, J. Magnin, Z. Rácz, and M. Zrinyi, *J. Chem. Phys.* **109**, 9479 (1998).
- [19] C. Léger, F. Argoul, and M. Bazant, *J. Phys. Chem. B* **103**, 5841 (1999).
- [20] C. N. Baroud, F. Okkels, L. Ménétrier, P. Tabeling, *Phys. Rev. E* **67**, 060104 (2003).
- [21] M. Chacron and I. L'Heureux, *Phys. Lett. A* **263**, 70 (1999).
- [22] J. W. Cahn and J. E. Hilliard, *J. Chem. Phys.* **28**, 258 (1958); *J. W. Cahn, Acta Metall.* **9**, 795 (1961).
- [23] The Cahn-Hilliard equation with additive conserved noise is the much studied Model B of critical dynamics [P. C. Hohenberg and B. I. Halperin, *Rev. Mod. Phys.* **49**, 435 (1977)].
- [24] A. Volford, I. Lagzi, F. Molnár, and Z. Rácz, *Phys. Rev. E* **80**, 055102(R), (2009).
- [25] J. D. Gunton, M. San Miguel, and P. S. Sahni, in *Phase Transitions and Critical Phenomena*, edited by C. Domb and J. L. Lebowitz (Academic, London, 1983), Vol. 8.
- [26] See Supplementary Information for a detailed model description, and for examples of three-dimensional simulations.
- [27] B. Chopard, P. Luthi, and M. Droz, *Phys. Rev. Lett.* **72**, 1384 (1994).
- [28] P. Hantz and I. Biró, *Phys. Rev. Lett.* **96**, 088305 (2006).
- [29] E. M. Foard and A. J. Wagner, *Phys. Rev E* **85**, 011501 (2012).
- [30] Z. Rácz, *Physica A* **274**, 50 (1999).
- [31] Computations for a 3D tube are also possible but exceedingly time consuming. An example of helicoid obtained in 3D is shown in [26].
- [32] S. Cornell and M. Droz, *Phys. Rev. Lett.* **70**, 3824, (1993).

SUPPLEMENTARY INFORMATION

**A. Detailed model description**

Liesegang patterns are formed in the wake of moving reaction-diffusion fronts. The reaction front emerges due to the inhomogeneous initial distribution of the reagents  $A$  and  $B$ . Namely, the reaction takes place in a gel occupying the half space  $x > 0$  where, initially, the inner electrolyte  $B$  is distributed homogeneously [ $b(x, y, t = 0) = b_0\theta(x)$ ]. The outer electrolyte  $A$  of much higher initial concentration [ $a(x, y, t = 0) = a_0\theta(-x)$  with  $a_0 \gg b_0$ ] is brought into contact with the gel at  $t = 0$ . Assuming a second-order, irreversible reaction  $A + B \rightarrow C$ , the front invading the gel is described by the equations

$$\partial_t a = D_A \Delta a - kab \quad (5)$$

$$\partial_t b = D_B \Delta b - kab \quad (6)$$

where  $k$  is the reaction rate and, for simplicity, the diffusion constants of the reagents are assumed to be equal ( $D_A = D_B = D$ ). This assumption will be used throughout the two-dimensional simulations.

The front, characterized by the spatio-temporal properties of  $kab$  (rate of production of  $C$ s), has been studied in detail [17, 18]. It is narrow and moves diffusively (its position is given by  $x_f = \sqrt{2D_f t}$  where  $D_f$  can be expressed through  $D$  and  $b_0/a_0$ ). It leaves behind a constant concentration,  $c = c_0$ , of the reaction product  $C$ , where the parameter  $c_0$  is determined by  $D$  and  $b_0/a_0$ , and is practically independent of  $k$ .

Assuming that no intermediate complexes are formed, the next stage of the formation of the precipitation pattern is the separation of the reaction product,  $C$ , into high- and low-concentration phases. At a coarse grained level, the phase separation can be described by the generalized Cahn-Hilliard equation [14, 22–24]

$$\partial_t c = \lambda_0 \Delta (\delta f / \delta c) + kab + \eta_{c0}. \quad (7)$$

Here  $\lambda_0$  is a kinetic coefficient,  $f$  is the free energy driving the phase separation,  $kab$  describes the creation of  $C$  particles by the front, and  $\eta_{c0}$  represents noise effects (thermal fluctuations, inhomogeneities in the gel, etc.) which conserve the total number of  $C$  particles.

In order to describe the phase separation, the free energy  $f(c)$  should have two minima corresponding to the low- ( $c_\ell$ ) and high ( $c_h$ ) concentrations of  $C$ s in homogeneous equilibrium states. It should also have a surface tension term preventing the formation of singularities at interfaces. As a convenient form with minimal number of parameters, one can take  $f$  as a Landau-Ginzburg free energy which is symmetric about  $\bar{c} = (c_h + c_\ell)/2$

$$f(c) = -\frac{\varepsilon}{2}(c - \bar{c})^2 + \frac{\gamma}{4}(c - \bar{c})^4 + \frac{\sigma_0}{2}(\nabla c)^2. \quad (8)$$

where  $\varepsilon$ ,  $\gamma$ , and  $\sigma_0$  are phenomenological parameters, and the minima of  $f(c)$  are fixed at  $c_h$  and  $c_\ell$  by setting  $\sqrt{\varepsilon/\gamma} = (c_h - c_\ell)/2 \approx c_h/2$  where we use the fact that  $c_h \gg c_\ell$  i.e. the gaps between the bands have very low steady-state concentration of  $C$ s in the usual Liesegang experiments.

Measuring concentration, time, and length in units of

$$\hat{c} = \frac{c_h - c_\ell}{2} \approx \frac{c_h}{2}, \quad \tau = \frac{1}{k\hat{c}}, \quad l = \sqrt{\frac{D}{k\hat{c}}} \quad (9)$$

and, furthermore, making a shift in the concentration of  $C$ s

$$m = \frac{c - (c_h + c_\ell)/2}{(c_h - c_\ell)/2} \approx \frac{c}{\hat{c}} - 1 \quad (10)$$

one obtains a simple set of equations

$$\partial_t a = \Delta a - ab \quad (11)$$

$$\partial_t b = \Delta b - ab \quad (12)$$

$$\partial_t m = -\lambda \Delta (m - m^3 + \sigma \Delta m) + ab + \eta_c, \quad (13)$$

where  $\lambda = \lambda_0 \varepsilon / D$ ,  $\sigma = \sigma_0 k \hat{c} / D \varepsilon$ ,  $\eta_c = \eta_{c0} / k \hat{c}^2$  are the rescaled kinetic coefficient, surface tension, and conserved noise, respectively.

A few comments are in order about the random aspects of the dynamics. First, we note that randomness is not added to the reaction-diffusion equations (11,12) since the noise has been shown to be irrelevant in determining the properties of the  $A + B \rightarrow C$  type reaction fronts in the physically relevant dimensions [32]. Second, we recall that the noise term  $\eta_c$  in the generalized Cahn-Hilliard equation (Model B [23]) describes the local concentration-fluctuations resulting from diffusive random motion of  $C$ s. This noise conserves the total number of particles and is expected to be proportional to  $\sqrt{\bar{c}}$ . Third, we point out that the amplitude of  $\eta_c$  in near-equilibrium dynamics is proportional to the temperature and it is related to the kinetic coefficient  $\lambda$ . However, we have here a far from equilibrium situation, and no fluctuation-dissipation relation connects these parameters. Accordingly, we shall treat  $\lambda$  and the amplitude  $\eta$  of  $\eta_c$  as independent parameters. Of course, one expects that temperature is related to the noise and, in general,  $\eta$  increases with temperature. In the simulations, the discretized noise term [ $\eta_c$  in (13)] was implemented by moving  $C$ s between neighboring sites at a rate proportional to  $\eta_c = \sqrt{\bar{c}}r$  where  $r$  is a uniformly distributed random number from the interval  $[-\eta, \eta]$ , and  $\eta$  is the parameter which is called the amplitude of the noise.

The above formulation is remarkable in that the number of parameters ( $\lambda, \sigma, \eta$ ) is small compared to that found in the usual models of Liesegang phenomena.

Among the parameters,  $\sigma$  does not appear to be important since it just determines the width of the transition between the high- and low-concentration regions. The parameter  $\lambda$ , on the other hand, does play an essential role since it sets the timescale of the precipitation processes. Comparing this timescale with the time the front passes through a region determines whether the nucleation-and-growth or the unstable growth (spinodal decomposition) modes dominate the phase separation dynamics. Finally, the noise  $\eta_c$  is also important. First, because the formation of helices is a symmetry breaking process which does not happen without the presence of noise. Second, because it determines the phase diagram (the meta- and unstable regions) for the given parameter values of the system.

Unfortunately, the parameters  $\lambda, \sigma, \eta$  are not easily controlled in experiments. For example, when trying to amplify  $\eta$  by increasing the temperature, one immediately realizes that there are a number of parameters (diffusion coefficients, reaction rate, etc.) which have strong but largely unknown temperature-dependence with unpredictable combined effects.

The parameters which are controllable in the experiments come from the initial preparation of the systems. They are the initial concentrations of the electrolytes ( $a_0, b_0$ ) and, furthermore, it turns out that the radius  $R$  of the test tube also sets some constraints on the emergence of helices.

### B. Additional information about the simulations

The solution of the discretized equations (11-13) with the above boundary and initial conditions were carried out using a uniform grid with various combination of scaled  $L_x$  and  $L_y$  from the ranges of  $32 \leq L_y/l \leq 512$  and  $512 \leq L_x/l \leq 2048$ . The equations were integrated in time by the simple Euler method (fast and extensive search in the parameter space was feasible by using the parallel programming possibilities of video cards). For the results quoted and displayed in the paper, the grid

spacing and the time step were 1.0 and 0.02, respectively.

### C. Three-dimensional simulations

Three-dimensional systems can also be studied by simulating the  $d = 3$  versions of equations (5-7). There are two changes compared to the  $d = 2$  case. First, in order to be in agreement with the experimental setup, the periodic boundary conditions are replaced by no-flux boundary conditions in the direction perpendicular to the direction of motion of the front. Second, we lift the restriction of  $D_A = D_B$  in our search for helicoids, and this means that an additional parameter  $\theta = D_A/D_B$  appears in the scaled equations.

In the simulations, we find that both the Liesegang and the helicoidal patterns observed in the experiments can be qualitatively reproduced (see Fig.5). Unfortunately, the time-scale of the simulations compared to the  $d = 2$  ones is multiplied roughly by  $2R$  where  $R$  is the scaled radius of the tube (the grid spacing used was 1.0). As a consequence, the computer power presently available to us is insufficient for obtaining good quality statistics for the probability of helicoid formation in  $d = 3$ .

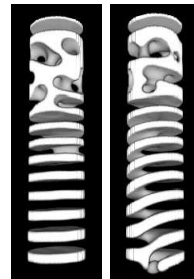


FIG. 5: Precipitation patterns (Liesegang on the left, helicoidal on the right) obtained in  $d = 3$  simulations using the following scaled parameters  $a_0 = 100$ ,  $b_0 = 1$ ,  $\sigma = 0.8$ ,  $\lambda = 0.2$ ,  $\eta = 0.02$ ,  $\theta = 1.2$ , and  $R = 24$ . The only difference in the simulations is the initial seed for the random number generator.